

Strong Electron-Phonon coupling in High Temperature Superconductors.

A. Lanzara*†, P. V. Bogdanov*, X. J. Zhou*, S. A. Kellar*, D. L. Feng*, E. D. Lu†, T. Yoshida‡, H. Eisaki*, A. Fujimori‡, K. Kishio§, J. -I. Shimoyama§, T. Noda||, S. Uchida||, Z. Hussain†, and Z.-X. Shen*.

**Department of Physics, Applied Physics and Stanford Synchrotron Radiation Laboratory, Stanford University, Stanford, CA 94305.*

†Advanced Light Source, Lawrence Berkeley National Lab., Berkeley, CA 94720.

‡Department of Physics, University of Tokyo, Bunkyo-ku, Tokyo 113, Japan.

§Department of Applied Chemistry, University of Tokyo, Tokyo 113-8656, Japan.

||Department of Superconductivity, University of Tokyo, Yayoi2-11-16, Bunkyo-ku, Tokyo 113, Japan.

The identification of phonon anomalies in the electronic tunneling spectra played a decisive role in our understanding of conventional superconductors¹. Recently an abrupt change in the electronic quasiparticle dispersion near (50 ± 15) meV binding energy has been observed in angle resolved photoemission spectroscopy (ARPES) from $\text{Bi}_2\text{Sr}_2\text{CaCu}_2\text{O}_8$ (Bi2212)²⁻⁴. This behavior indicates a many-body effect likely to be very important for the physical properties and pairing mechanism. While two groups have positively identified this effect^{2,3}, there is no consensus on the origin of the feature: with phonons, the magnetic resonance mode and energy gap as possible candidates. This paper reports new data revealing the following behavior of this effect: a) it has an energy scale of 50-80 meV and is ubiquitous in hole doped materials; b) the effect is seen well above the critical temperature (T_c); c) the coupling gets weaker with increasing doping; d) the momentum dependence of the effect is weak. These results rule out both the magnetic resonance mode and energy gap as possible explanations, leaving phonons as the only surviving candidate.

To conclusively characterize the many-body effect seen in the quasiparticle dispersion it is necessary to carry out doping, momentum and temperature (above and below T_c) dependent analysis. In this paper we report a detailed study of the electronic quasiparticle dispersions from three different families of p-type cuprates, Bi2212 and Pb doped Pb-Bi2212, Pb-doped $\text{Bi}_2\text{Sr}_2\text{CuO}_6$ (Bi2201) and $\text{La}_{2-x}\text{Sr}_x\text{CuO}_4$ (LSCO). The experimental details are reported in ref. 5.

The top panels of figure 1 report the momentum distribution curve (MDC) derived dispersions along the $(0, 0)-(\pi, \pi)$ direction for LSCO (panel a), Bi2212 superconducting state (panel b) and Bi2201 normal state (panel c) vs the rescaled momentum, k' , defined by normalizing to one the $(k-k_F)$ vector at $E=170\text{meV}$. The “kink” in the dispersion around 50-80meV, highlighted by thick arrows in the figure, is

the many-body effect of interest^{2,3}. The direct comparison suggests a similar phenomenon in different systems (although details differ) and at different doping with the effect gets stronger in the underdoped region. These results put a strong constraint on the nature of the effect. The similar energy scale of the excitation (50-80 meV) in systems with very different gap energy, ranging from (10-20 meV) for LSCO and Bi2201, to (40-50meV) for Bi2212, rules out the superconducting gap as the origin. The data also rule out the proposed explanation⁶ in terms of coupling with the magnetic mode at 41meV, because of its temperature dependence and its ubiquity. This includes the observation of this phenomenon in systems such as LSCO where the magnetic mode does not exist, and well above the critical temperature, as the magnetic mode sets in at T_c for optimal and overdoped samples⁷ (e.g. the 30K data from overdoped Bi2201 are measured at six times the T_c). These straightforward considerations, based on direct experimental evidences, leave phonons as the only possible candidate.

The phonon interpretation receives very strong support from a direct comparison between photoemission results and the phonon dispersion, as determined by neutron scattering in the case of LSCO, for which both sets of data are available. As shown by the red arrow and the shaded area in Fig. 1a, the energy of the zone boundary in-plane oxygen stretching LO phonon, identified by neutron as being strongly coupled to charge^{8, 9}, coincides almost perfectly with the “kink” energy in our data. Additional support for the phonon scenario also comes from a temperature dependence analysis. In the lower panel, we report the evolution of the kink above and below the critical temperature for LSCO (panel d) and Bi2212 (panel e). In both cases the kink persists clearly above the critical temperature as expected in the case of electron-phonon interaction, however a thermal broadening is present.

Fig. 2 compares energy distribution curve (EDC) data of Pb-Bi2212 along (0, 0)-(π , π), and (0, 0)-(π , 0) directions (panel a-b), with that of Be (0001) surface state¹⁰, in which

the electron-phonon interaction is known to be strong (panel c), and also with simulated spectra (panel d). The locations of the labeled EDC spectra near the Fermi surface in figure 2a and 2b, are indicated by filled circles in the inset of figure 4b. A strong similarity among the raw data can be observed. In the case of Be, the 60meV phonon sets a scale below which a sharp quasiparticle is possible. This leads to a “dip” or “break” in the spectra near the phonon energy, indicated by the vertical dashed line. This feature is well reproduced in the simulation, where a quasiparticle is isotropically coupled to a collective mode near 70meV^{6,11}. The Pb-Bi2212 data show also a clear resemblance, with a phonon near 70meV^{8,9}. Therefore, the observed spectral lineshapes are also consistent with the phonon explanation.

In Fig. 3a we report the quasiparticle width of Bi2212 for different doping, using a typical procedure². As shown before^{2,3} the width decreases more rapidly below the relevant energy, which corresponds to the kink position in the dispersion. This again is consistent with the case of an electron-phonon coupled system, complementing dispersion data in Fig. 1. The drop in the scattering rate near the relevant energy is also seen in optics experiments¹². Fig. 3b reports the “dip” energy of ARPES spectra near $(\pi, 0)$ as a function of doping. The data are consistent with the LO phonon energy which sets the lower bound. A realistic model, which considers the change of the $(\pi, 0)$ band position with doping, electron-phonon interaction and many-body effects, will be needed to understand the specifics of the data, including the small decrease of the dip energy with doping. However, the data show a consistency between photoemission and neutron results on phonons.

In a simple electron-phonon model the ratio of the velocity change, between the dressed and the bare electrons velocity is $(\lambda' + 1)$, where λ' measures the electron-phonon coupling strength. We can extract a similar quantity from the ratio between the bare quasiparticle velocity (which in this case is approximated by the high energy part of the

dispersion, above the phonon energy) and the dressed velocity (below the phonon energy). The two velocities are extracted fitting the experimental dispersions with two straight lines. In Fig. 1f we report the doping dependence of the electron-phonon coupling strength λ' . Given $\lambda' \sim 1-1.5$ the electron-phonon coupling is strong, in optimal and underdoped case.

In figure 4, panel a, we report the velocity ratio $(\lambda' + 1)$ for different materials, as a function of the angle ϕ ¹³ along the entire FS (panel b). Samples of angular dependent data are shown in Fig.1b, Fig.2 and Fig. 4b. Data obtained from different experimental runs are included in the figure (full and empty symbols). In panel b) we report the rescaled MDC derived dispersions for Pb-Bi2212 along the two high symmetry directions, ΓY $((0, 0) - (\pi, \pi))$ and ΓM $((0, 0) - (\pi, 0))$. The total change in the ratio is slightly less than a factor of two. In particular, the data from both Pb-doped Bi2212 and Pb-doped Bi2201, where the superstructure effect near $(\pi, 0)$ is minimized, gives confidence to the conclusion (consistent results are also seen in LSCO). No direct relation with the superconducting transition is observed, as can be seen in the same figure where data above (100K) and below (20K) the critical temperature are reported in the case of Pb-doped Bi2212. Both the angular and the temperature dependence are consistent with the phonon interpretation, as phonons are more isotropic and will not disappear above T_c .

While these experimental findings points toward phonons as the only possible scenario, some literature needs to be addressed. Eschrig and Norman⁶ attributed the kink in the dispersion along the (π, π) direction and the dip in the EDCs near $(\pi, 0)$ to the magnetic mode of 41 meV⁷. Comparing the doping dependence of the energy difference between the dip and the superconducting gap in photoemission data, with that of the magnetic mode in neutron data, Campuzano et al.¹⁴ claimed a definitive proof for the (π, π) resonance mode as the origin of the “peak-dip-hump” structure. Valla et al.⁴ on the other

hand, argued for the absence of an energy scale in the problem and that the kink is not due to phonons¹⁵. They attribute the curving in the normal state dispersion to the marginal Fermi liquid (MFL) self-energy¹⁶, and the presence of a sharp kink below T_c to coupling to the (π, π) magnetic mode¹⁷.

Aside from its incompatibility with our data, the (π, π) mode scenario has serious weaknesses. First, the mode contains only few percent of the total spin fluctuation spectral weight^{18,19}, unlikely an explanation for the very large change seen in EDC spectra above and below T_c . Second, the electronic model is difficult to implement self-consistently as the mode will be altered by the interaction with electrons⁶. Third, the magnetic mode calculation claims to reproduce the experimental data by Kaminski et al³, that would yield an unreasonably large coupling constant ($\lambda' \sim 30$). The inset of Fig. 4a compares the velocity ratio found in the present study with the data by Kaminski et al³. The comparison shows good agreement for $\phi \leq 30$ degree, but a large discrepancy is observed for $\phi \geq 30$ degree, with the Kaminski data yielding a very large coupling constant (~ 30) near $(\pi, 0)$ region. We attribute this difference to confusion caused by the superstructure, which complicates the data near $(\pi, 0)$ region in pure Bi2212 sample used by Kaminski et al³. We have chosen superstructure free Pb-Bi2212 for this investigation.

The above discussion rules out the (π, π) mode as a possible scenario, and this makes also the MFL plus (π, π) mode interpretation an unnatural explanation for the data showing a sharper kink below T_c . Furthermore, some of the normal state dispersion, for example the 7% underdoped LSCO (fig. 1a) measured at T_c where the kink is sharper, cannot be fit within the MFL approach, even with an arbitrary choice of parameters. If the 7% LSCO data can only be explained by coupling to phonons, it is likely that a similar effect, observed at higher doping and temperatures, requires the same cause. Finally, this attempt to attribute the “kink” in the dispersion, occurring at the same

energy above and below T_c to two different origins is not consistent with the data in Fig. 1e (inset) where one sees that the effect washes out gradually with temperature.

The phonon scenario can explain all the aspects of the data, attributed to the (π, π) mode, in a more natural way. Nagaosa et al²⁰ reproduced the observed ARPES results in the case of coupling to LO phonon, adapting a similar approach as the one used by Eschrig and Norman⁶. This calculation has the added advantage of not suffering from the tiny spectral weight and the self-consistency issue present in the magnetic mode calculation. The doping dependence of the energy difference between the dip and the peak position can be as well understood in the phonon context, if the doping and momentum dependence of the phonon energy, the coupling strength and the superconducting gap are included. Unlike the MFL plus (π, π) mode scenario, the phonon picture naturally explains the gradual temperature evolution observed in the MDC derived dispersions. The change in the EDCs below T_c can be explained by the emergence of a quasiparticle below T_c , that reveals the peak-dip-hump structure, which is hard to resolve above T_c .

In summary new ARPES data from three families of p-type cuprates provide compelling evidence for strong electron-phonon coupling. This result suggests that phonons are an important player for the physics of cuprates.

1. Scalapino, D. J., Schrieffer, J. R. & Wilkins, J. W. Strong-Coupling Superconductivity. *Phys. Rev.* **148**, 263 (1966).
2. Bogdanov, P. V. et al. Evidence for an Energy Scale for Quasiparticle Dispersion in $\text{Bi}_2\text{Sr}_2\text{CaCu}_2\text{O}_{8+\delta}$. *Phys. Rev. Lett.* **85**, 2581-2584 (2000).
3. Kaminski, A. et al. Renormalization of spectral lineshape and dispersion below T_c in $\text{Bi}_2\text{Sr}_2\text{CaCu}_2\text{O}_{8+\delta}$. *cond-mat* 0004482 (2000).
4. Valla, T. et al. Evidence for Quantum Critical Behavior in the Optimally Doped Cuprate $\text{Bi}_2\text{Sr}_2\text{CaCu}_2\text{O}_{8+\delta}$. *Science* **285**, 2110-2113 (1999).
5. The Pb substituted Pb-Bi2212, $\text{Bi}_2\text{Sr}_2\text{CuO}_6$ (Pb-Bi2201) (overdoped, $T_c=7\text{K}$) and $\text{La}_{2-x}\text{Sr}_x\text{CuO}_4$ (LSCO) data, in figures 1, 2, 4, have been recorded at beam-line 10.0.1.1 of the Advanced Light Source (ALS), utilizing 55 eV photon energy, as reported before². The Pb-Bi2201 (overdoped, $T_c=5\text{K}$) data have been recorded at the beam-line 5.4 of the Stanford Synchrotron Radiation Laboratory (SSRL). Except SSRL 5-3 data, in fig. 3b, all spectra were collected using Scienta SES 200 spectrometer. The vacuum during the measurements was better than 6×10^{-11} Torr. Unless specified, the overdoped (OD) Pb-Bi2212 ($T_c=82.5\text{K}$; Pb doping 11% of Bi sites); optimally doped (opt) Bi2212 ($T_c=91\text{K}$), underdoped (UD) Bi2212 ($T_c=84\text{K}$), and LSCO samples (OD ($x=0.22$), opt. ($x=0.15$) and UD ($x=0.07$)), were measured at 20K and 100K. The Pb-Bi2201 samples (OD $T_c=7\text{K}$ and $T_c=5\text{K}$) were measured at 30K.
6. Eschrig, M. & Norman, M. R. Neutron Resonance: Modeling Photoemission and Tunneling Data in the Superconducting State of $\text{Bi}_2\text{Sr}_2\text{CaCu}_2\text{O}_{8+\delta}$. *Phys. Rev. Lett.* **85**, 3261-3264 (2000).

7. He, H. et al. Resonant Spin Excitation in an Overdoped High Temperature Superconductor. *cond-mat* 0002013 (2000).
8. McQueeney, R. J. et al. Anomalous Dispersion of LO Phonons in $\text{La}_{1.85}\text{Sr}_{0.15}\text{CuO}_4$ at Low Temperatures. *Phys. Rev. Lett.* **82**, 628-631 (1999).
9. Petrov, Y. et al. Phonon Signature of Charge Inhomogeneity in High Temperature Superconductors $\text{YBa}_2\text{Cu}_3\text{O}_{6+x}$. *cond-mat* 0003414 (2000).
10. Hengsberger, M., Purdie, D., Segovia, P., Garnier, M. & Baer, Y. Photoemission Study of a Strongly Coupled Electron-Phonon System. *Phys. Rev. Lett.* **83**, 592-595 (1999).
11. Scalapino, D. J. in *Superconductivity*, edited by R. D. Parks (Marcel Dekker, NY 1969) pp. 449; and references therein.
12. Puchkov, A. V. Basov, D. N, Timusk, T. The Pseudogap State in High T_c superconductors: An infrared study. *J. Phys. Condens. Matter* **8**, 10049-10082 (1996).
13. The angle ϕ along the FS is defined as the angle between the Γ -Y $((0, 0)-(\pi, 0))$ line and the line from Γ $((0, 0))$ to the point on the Fermi surface we are considering. The cut are always normal to the experimentally determined Fermi surface.
14. Campuzano, J. C. et al. Electronic Spectra and Their Relation to the (π, π) Collective Mode in High- T_c Superconductors. *Phys. Rev. Lett.* **83**, 3709-3712 (1999).
15. Valla, T. et al. Charge-Density-Wave-Induced Modifications to the Quasiparticle Self-Energy in 2H-TaSe₂ *Phys. Rev. Lett.* **85**, 4759-4762 (2000).

16. Varma, C. M., Littlewood, P. B., Schmitt-Rink, S., Abrahams, E., and Ruckenstein, A. E. Phenomenology of the normal state of Cu-O high-temperature superconductors. *Phys. Rev. Lett.* **63**, 1996-1999 (1989).
17. Johnson, P. D. presentation at ASPEN Winter Conference on Superconductivity, January 2001.
18. Demler, E. and Zhang, S.-C. Quantitative test of a microscopic mechanism of high-temperature superconductivity. *Nature* **396**, 733-735 (1998); and references therein.
19. Fong, H. F. et al. Polarized and unpolarized neutron scattering study of the dynamic spin susceptibility in $\text{YBa}_2\text{Cu}_3\text{O}_7$. *Phys. Rev. B* **54**, 6708-6720 (1996).
20. Nagaosa, N. et al. *unpublished*.
21. Ding, H. et al. Coherent quasiparticle weight and its connection to high- T_c superconductivity from angle-resolved photoemission. *cond-mat* 0006143 (2000).
22. Renner, C. H. et al. Pseudogap Precursor of the Superconducting gap in under- and overdoped $\text{Bi}_2\text{Sr}_2\text{CaCu}_2\text{O}_8$. *Phys. Rev. Lett.* **80**, 149-152 (1998); Observation of the low Temperature pseudogap in the vortex core of $\text{Bi}_2\text{Sr}_2\text{CaCu}_2\text{O}_8$. *ibid.* **80**, 3606-3609 (1998).
23. Cren, T. et al. Influence of Disorder on the Local Density of States in High- T_c Superconducting Thin Films. *Phys. Rev. Lett.* **84**, 147-150 (2000).
24. De Wilde Y. et al. Unusual Strong-Effects in the Tunneling Spectroscopy of Optimally Doped and Overdoped $\text{Bi}_2\text{Sr}_2\text{CaCu}_2\text{O}_8$. *Phys. Rev. Lett.* **80**, 153-156 (1998).

We acknowledge N. Nagaosa, D. J. Scalapino, R. Laughlin, D.-H. Lee, S. Kivelson, D. Bonn, N. P. Armitage, A. Damascelli and F. Ronning for useful discussion. The work at ALS was supported by DOE's Office of Basic Energy Science, Division of Materials Science with contract DE-AC0376SF00098. The SSRL's work was also supported by the Office Division of Materials Science. The Stanford work was also supported by NSF grant DMR-9705210. One of us A.L. would like to thank the Istituto Nazionale Fisica della Materia (INFM).

Correspondence and requests for materials should be addressed to: Z-X. Shen (e-mail: zxshen@stanford.edu).

Figure 1: In the top panels the MDCs derived dispersions along $(0, 0)$ - (π, π) (except inset of panel b, which is off this line) vs the rescaled momentum k' for different samples and different doping are reported. Panel a) shows the doping dependence of LSCO (at 20K), panel b) Bi2212 samples (superconducting state, 20K) and panel c) of Bi2201 (normal state, 30K). The dotted lines in the figures are guides to the eye. The kink position in panel a) is compared with the phonon energy at $q=(\pi, 0)$ (thick red arrow) and the phonon dispersion (shaded area) from neutron data⁸. The doping was determined from the T_c vs doping universal curve. In the inset of panel b) we report the dispersions off the $(0, 0)$ - (π, π) direction, showing a clear sharpening of the kink upon moving away from the nodal direction. The black arrows indicate the position of the kink in the dispersions. The temperature dependence of the dispersions is reported in the lowest panels for both LSCO (panel d, optimally doped) and Bi2221 (panel e, optimally doped). In the inset of panel e) the difference spectra, with respect to the lower temperature (20K), are reported. In panel f) the doping dependence of the el-ph coupling constant, λ' , along $(0, 0)$ - (π, π) direction is shown as a function of doping. Data for the LSCO (full triangles) and NdLSCO (1/8 doping) (full diamond), Bi2201 (full squares) and Bi2212 (full circles) samples are reported. The different colors represents data obtained in different experimental runs. The shaded area is a guide to the eyes.

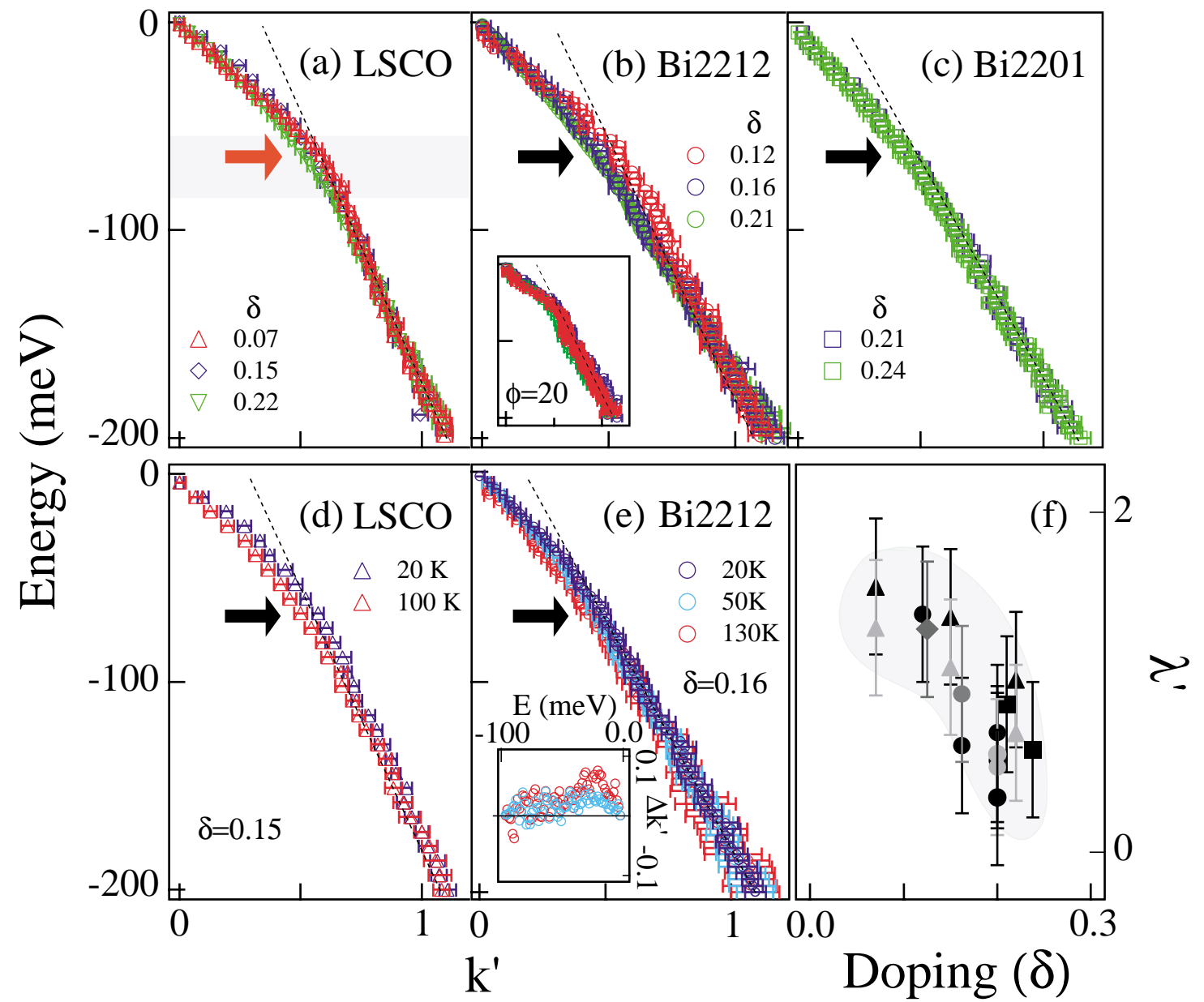
Figure 2: Raw EDCs for the overdoped Pb-Bi2212 at low temperature ($T=20K$) are reported in panel a), cut along the nodal $(0, 0)$ - (π, π) direction, ($\Phi=0^\circ$), and in panel b), cut along the $(0, 0)$ to $(\pi, 0)$ direction, ($\Phi=45^\circ$). In panel c) the raw EDCs for the Be(0001) surface¹⁰ are shown. In panel d) EDCs of simulated spectra, obtained in the simple case of an isotropic coupling to a single phonon mode, are shown. A straight line highlights the zero energy position and a dashed line highlights the known phonon energy⁸. The relative k locations of the

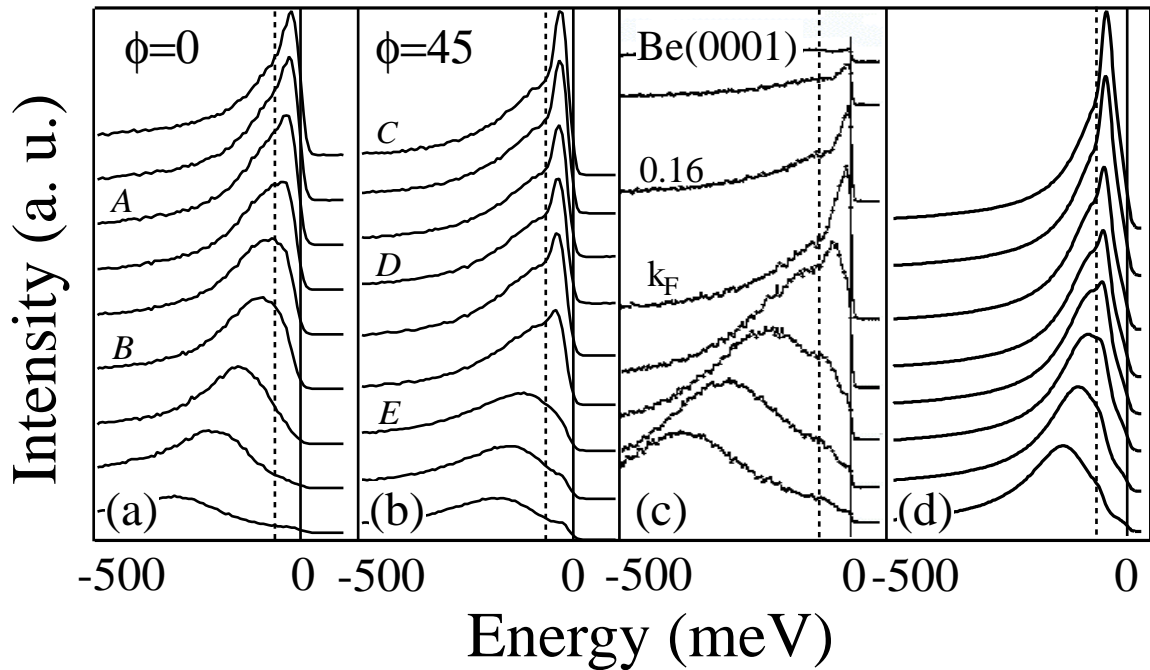
individually labeled spectra in panels a) and b), are indicated in the inset of figure 4b) by filled circles along the two high symmetry directions.

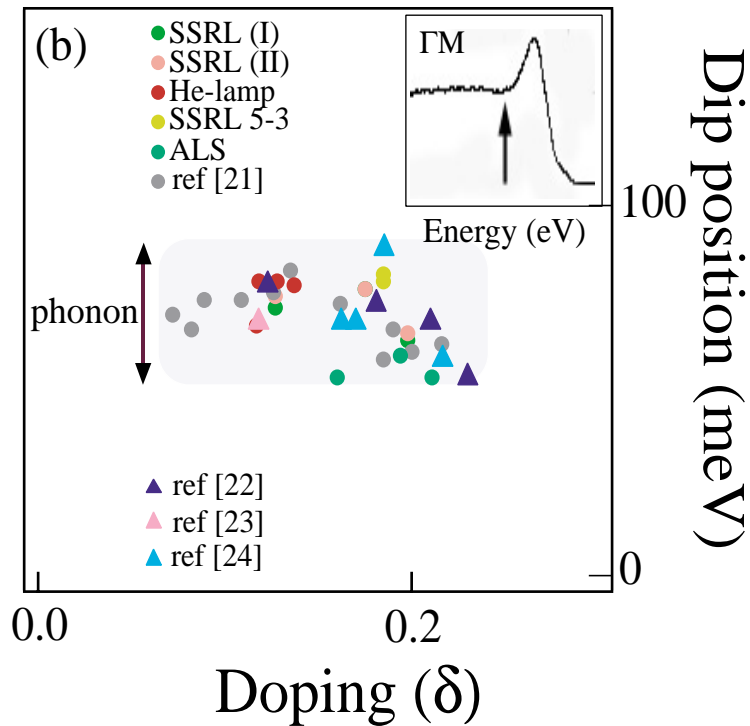
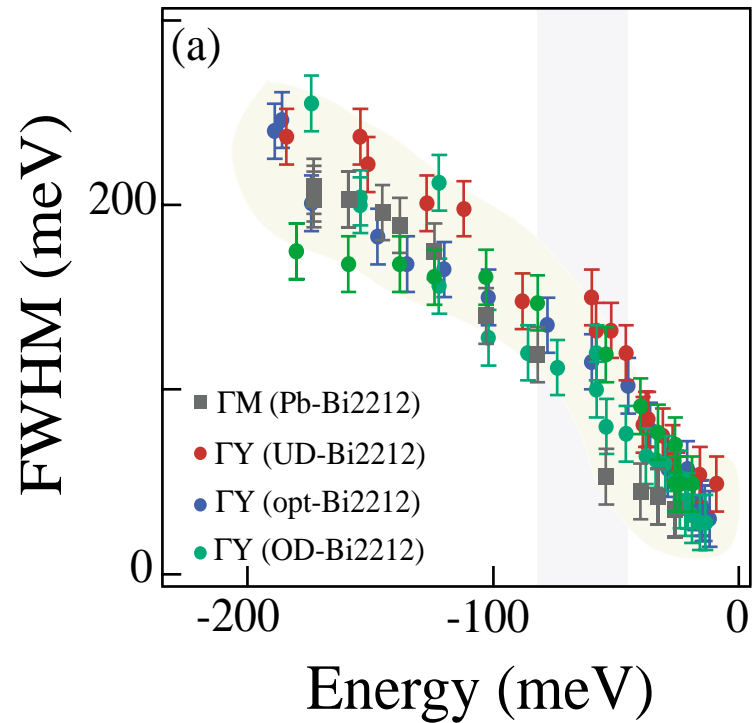
Figure3: Panel a) reports the quasiparticle width along the ΓY $((0, 0)-(\pi, \pi))$ (circles) for Bi2212 and Pb-Bi2212, and along ΓM $((0, 0)-(\pi, 0))$ (squares) direction, for the superstructure free Pb-Bi2212 system. In panel b) the doping dependence of the dip position for the Bi2212 samples, near the $(\pi, 0)$ region is reported, as indicated in the inset of the same panel by the arrow. The dip position has been obtained both from photoemission (circles) and tunneling data (triangles²²⁻²⁴). The photoemission data have been collected at SSRL, beam-line 5.4 in transmission mode (I) (green circles) and angular mode (II) (pink circles) and at SSRL, beam line 5.3 (yellow circles). The data at ALS are collected in angular mode (light green circles). Red circles represent the He-lamp data, collected with a Scienta analyzer. Our data are compared with data points from ref. 21 (gray circles). The shaded region in panel b) represents the phonon energy, including dispersion and width⁸.

Figure 4: In the inset of panel b) the location of the cuts in the Brillouin zone are shown. Φ is defined as the angle between the Γ -Y line and the line from Γ to the point on the Fermi surface considered. Panel a) reports the velocity ratio $(\lambda'+1)$ vs angle ϕ along the FS. The empty and full symbols represent the values obtained fitting the MDCs dispersions in different experimental run. HT and LT indicate the values of the coupling constant obtained above and below the critical temperature. The HT data for the Pb-Bi2212 are collected at 100K (red circle) while the LT data at 20K (blue circle). The HT data for the Pb-Bi2201 system (squares) are collected at 30K. The LT data (at 20K) along the nodal direction, for the LSCO and NdLSCO systems are also included (empty yellow and full grey triangles). All velocity ratios are obtained for cuts perpendicular to

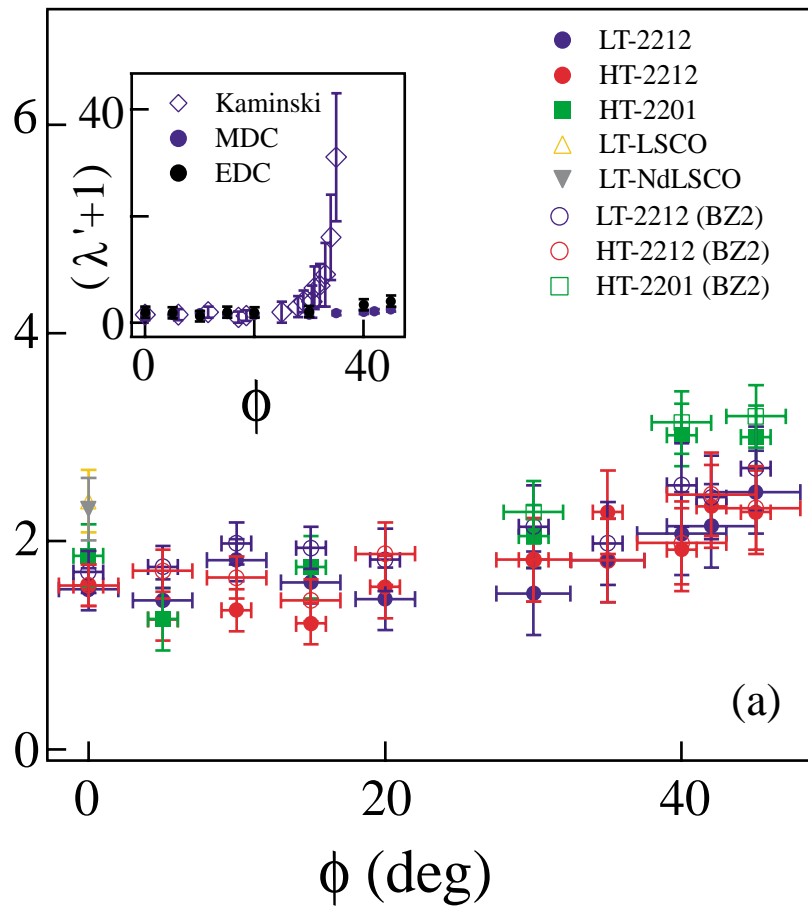
the FS at given ϕ . The inset of panel a) compares the $(\lambda'+1)$ value for the Pb-Bi2212 as obtained both from MDC (blue filled circles) and EDC (black filled circles), with data by Kaminski et al.³ on pure Bi2212 (empty diamonds). In panel b) the rescaled MDC derived dispersions, along the nodal and anti-nodal directions are shown for the Pb-Bi2212. The small deviation, above the phonon energy (indicated by the thick arrow), is caused by the difference in dispersion along the two directions.



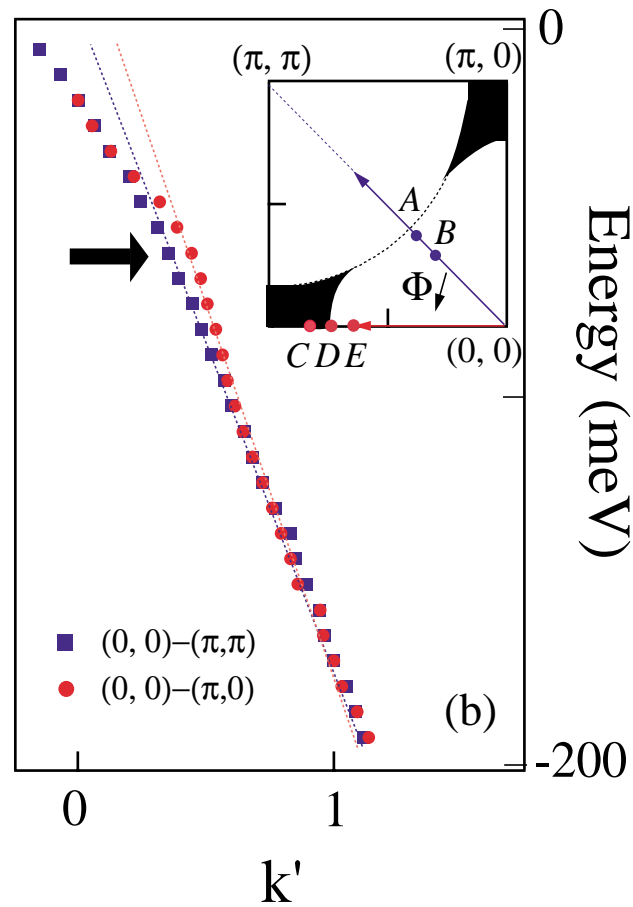




Velocity ratio ($\lambda'+1$)



(a)



(b)